Analytical and Bioanalytical Chemistry
https://doi.org/10.1007/s00216-020-02750-1

RESEARCH PAPER

Picomolar-level detection of mercury within non-biological/biological aqueous media using ultra-sensitive polyaniline-Fe_3O_4-silver diethyldithiocarbamate nanostructure

Seyyed Alireza Hashemi[1,2] · Seyyed Mojtaba Mousavi[2,3] · Sonia Bahrani[2] · Seeram Ramakrishna[1] · Seyyed Hamid Hashemi[2]

Received: 4 May 2020 / Revised: 18 May 2020 / Accepted: 29 May 2020

Abstract

Mercury as the 3rd most toxic, non-biodegradable, and carcinogenic pollutant can adversely affect the ecosystem and health of living species through its bioaccumulation within the nature that can affect the top consumer in the food chain; therefore, it is vital to sense/remove Hg^{2+} within/from aqueous media using practical approaches. To address this matter, we modified the glassy carbon electrode (GCE) with ultra-sensitive, interconnected, sulfurized, and porous nanostructure consisted of polyaniline-Fe_3O_4-silver diethyldithiocarbamate (PANi-F-S) to enhance the sensitivity, selectivity, and limit of detection (LOD) of the sensor. Obtained results showed that at optimum conditions (i.e., pH value of 7, deposition potential of − 0.8 V, and accumulation time of 120 s), for Hg^{2+} concentration ranging from 0.4 to 60 nM, the modified electrode showing linear relative coefficient of 0.9983, LOD of 0.051 nM, LOQ of 0.14 nM, and sensitivity of 1618.86 μA μM^{-1} cm^{-2} highlights superior sensitivity of the developed platform until picomolar level. Additionally, the modified electrode showed ideal repeatability, stability, reproducibility, and selectivity (by considering Zn^{2+}, Cd^{2+} Pb^{2+}, Cu^{2+}, Ni^{2+}, and Co^{2+} as metal interferences) and recovered more than 99% of the Hg^{2+} ions within non-biological (mineral, tap, and industrial waters) and biological (blood plasma sample) fluids.

Keywords Mercury · Sensor · Biosensor · Polyaniline · Diethyldithiocarbamate

Introduction

Superior toxicity of heavy metals has caused increasing concerns in the case of health, nutritional, genetic, and ecological matters [1]. Among these heavy metals, mercury ion (i.e., Hg^{2+}) is known as one of the most toxic heavy metals within the ecosystem which is non-biodegradable, highly carcinogenic, and highly toxic for the nervous system which can adversely affect the physiological performance of the human body, where the US Agency for Toxic Substances and Disease Registry (ATSDR) marked mercury as the 3rd most toxic element for public health [2–5]. Mercury can easily accumulate within the aquatic ecosystem and via its bioaccumulation process, it transfers its severe toxicity from the aqueous media to the top consumer in the food chain [6]. Exposure to diverse dosages of mercury can lead to severe adverse effects on the human body including cognitive disorder, brain damage, motion/neuro disorder, cancer, kidney failure, liver dysfunction, and distribution within the endocrine system [7]. According to the Environmental Protection Agency's statement, the highest allowed dosage of mercury within drinking water must not exceed 10 nM; therefore, it is vital to develop state-of-the-art detection platforms capable of detecting

Electronic supplementary material The online version of this article (https://doi.org/10.1007/s00216-020-02750-1) contains supplementary material, which is available to authorized users.

✉ Seyyed Alireza Hashemi
sa_hashemi@sums.ac.ir

[1] Department of Mechanical Engineering, Center for Nanofibers and Nanotechnology, National University of Singapore, Singapore 119260, Singapore

[2] Department of Medical Nanotechnology, School of Advanced Medical Sciences and Technologies, Shiraz University of Medical Sciences, Shiraz 71348-14336, Iran

[3] Department of Chemical Engineering, National Taiwan University of Science and Technology, Taipei City 10607, Taiwan

Published online: 06 June 2020

Table 1 Disease resulting from exposure to toxic heavy metals

Element	Symbol	ATSDR rank	Resulting disease	Ref.
Arsenic	As	1	Can cause peracute toxicity that leads to rapid death in few minutes/hours upon exposure to high dosage; direct exposure can lead to bladder, lung, skin, and kidney cancer. Also, it can severely change the color of the skin and leads to blackfoot disease.	[9, 10]
Lead	Pb	2	Inhabitation of enzyme function, changing the metabolism of vitamin D, deterioration of brain function, and known as a serious neurotoxicant. It can also lead to stroke, cancer, and heart disease.	[11–13]
Mercury	Hg	3	Adversely affect the performance of nervous, cardiovascular, renal, gastrointestinal, and hematopoietic systems. Mercury can cause genotoxicity, carcinogenicity, immunotoxicity, and endocrine along with severe developmental and reproductive toxicity.	[14–17]
Cadmium	Cd	7	Headache, sleep distribution, vertigo, tremor, sensory disturbance, and sweating are among the problems that associated via exposure with cadmium. Poisoning with cadmium can lead to itai-itai disease, softness of bones, kidney failure, and cancer (especially lung, prostate, breast, and kidney cancer).	[18–20]
Chromium, hexavalent	Cr(VI)	17	This chemical compound is highly genotoxic and carcinogenic and can lead to lung carcinogenesis. It can also lead to lung malignancies and its distribution in drinking water can lead to severe cancer within the small intestine and oral cavity. This chemical compound can cause ulcers and irritation in the intestines and stomach. It is also highly toxic for liver. Dyed textiles/leathers with this compound can cause serious skin allergy/sensitivity.	[21]

mercury at very low concentrations [8]. In Table 1, a list of the five most toxic heavy metals is presented, in which severe toxicity of these hazardous pollutants and their resulting illnesses are highlighted.

So far, diverse methods have been developed toward the accurate detection of mercury within aqueous media including electrochemistry [22–24], fluorescent [25], and colorimetry [26] methods, where despite their high selectivity and accuracy, most of these methods cannot be adapted for rapid and real-time detection of mercury within the aqueous media owing to their time-consuming and expensive approaches [27]. Among these methods, electrochemical approaches are considered the most promising detection method due to their low-cost, sensitive, dividable, easy-to-operate, and portable features [28]. In this matter, an unmodified electrode cannot show the desirable sensitivity and selectivity expected by drinking water standards; therefore, it is bare bone essential to develop practical nanostructures for improving the selectivity/sensitivity of the electrode [29].

This matter can be addressed through modification of electrodes with highly sensitive, selectable, and electroactive nanomaterials. Modified electrodes with advanced nanomaterials have been identified as most promising alternatives for accurate detection of mercury due to their large active surface area compared with their volume ratio, enhanced electrocatalytic performance, ideal surface properties, and superior absorption rate [30, 31]. In this case, diverse kinds of nanomaterials were developed and used for detection of mercury within aqueous media using diverse methods, where a list of recently developed electrodes and their limit of detection (LOD) is tabulated in Table 2.

In addition, in our recent research [45], we have modified polyaniline (PANi) with magnetite nanoparticles and silver diethyldithiocarbamate toward development of an interconnected, highly porous, and sulfur-rich nanostructure that can efficiently remove the three most toxic elements, i.e., arsenic, lead, and mercury, from aqueous media, where the outcome of Langmuir isotherm showed a new mile stone of about 222.2 and 175.4 mg g^{-1} for absorption of mercury and arsenic from aqueous media, respectively, for concentrations within the range of nanogram. In fact, outcome of this research revealed the superior sensitivity/activity of the developed platform against targeted pollutants which shows its potential for precise detection of these toxic elements within the aqueous ecosystem. In our previous study, we mainly focused on capabilities of developed nanostructures in particular of Hg, As, and Pb absorption, while in the current research, we highlighted/evaluated the potential of this superior absorber toward electrochemical detection of Hg within aquatic biological/non-biological media based on our recent achievements.

Table 2 A list of recently developed electrodes with advanced nanostructures toward accurate detection of mercury within aquatic media

Modified electrode	Method	Target pollutant	LOD (nM)	Ref.
HC/PCE	DPV	Hg^{2+}	8.0	[22]
GCE/Cu-Co HCF/$_L$-Cysteine	DPV	Hg^{2+}	80.0	[32]
GCE/Pd/PAC	DPV	Hg^{2+}	54	[33]
SPE/Bi NPs/G-CNT	DPV	Hg^{2+}	0.2	[28]
GCE/Pt/MZ	DPV	Hg^{2+}	3.4	[34]
GCE/PEE	DPV	Hg^{2+}	0.1	[35]
GCE/IIPN/MWCNT	DPASV	Hg^{2+}	5.0	[36]
PCE/IL/mesoporous silica	DPASV	Hg^{2+}	10.0	[37]
2,4,6-TMT/Au NPs	DPASV	Hg^{2+}	5.3	[38]
TiO_2-coupled Au	DPASV	Hg^{2+}	1.0	[39]
GCE/N-doped G	DPASV	Hg^{2+}	50	[40]
Au UMEA	LSV	Hg^{2+}	16	[41]
CNF or rGO/Au NPs	LSV	Hg^{2+}	30	[42]
Au film electrode	SC	Hg^{2+}	0.04	[43]
GCE/glycine	SWASV	Hg^{2+}	0.23	[44]
Au NP–decorated COF	CD	Hg^{2+}	0.75	[26]
ZnO NPs	Fluorescent	Hg^{2+}	20	[25]
ZnO ND	Fluorescent	Hg^{2+}	18	[25]
ZnO NR	Fluorescent	Hg^{2+}	35	[25]
ZnO NW	Fluorescent	Hg^{2+}	10	[25]
PANi-F-S	DPASV	Hg^{2+}	0.051	Current work

Abbreviations (modified electrode's section): *HC*, humic acid; *PCE*, paste carbon electrode; *GCE*, glassy carbon electrode; *PAC*, porous activated carbon; *SPE*, screen-printed electrode; *G-CNT*, graphene-carbon nanotube; *MZ*, mordenite zeolite; *PPE*, 1-phenyl-*N*-(pyridine-2-ylmethyl)ethanamine; *IIPN*, ion-imprinted polymeric nanobeads; *MWCNT*, multi-walled carbon nanotube; *IL*, ionic liquid; *2,4,6-TMT*, 2,4,6-trimercaptotriazine; *NPs*, nanoparticles; *N-doped G*, N-doped graphene; *UMEA*, ultra-microelectrode arrays; *CNF*, carbon nanofiber; *rGO*, reduced graphene oxide; *COF*, covalent organic framework; *ND*, nanodumbbell; *NR*, nanorod; *NW*, nanowire

Method's section: *DPV*, differential pulse voltammetry; *DPASV*, differential pulse anodic stripping voltammetry; *LSV*, linear sweep voltammetry; *SC*, stripping chronopotentiometry; *SWASV*, square wave anodic stripping voltammetry; *CD*, colorimetric detection

Herein, by considering the superior sensitivity and reactivity of PANi and dithiocarbamate-based materials as potential sensors for detection of heavy metals, e.g., Cu, Sb, Bi, Pb, As, and Hg [46–53], we developed the integrated platform of polyaniline-Fe_3O_4-silver diethyldithiocarbamate (PANi-F-S) as a modifying agent for enhancing the glassy carbon electrode (GCE). The modified electrode was used for real-time, selective, sensitive, accurate, repeatable, and picomolar-level detection of Hg^{2+} ions within aqueous and biological (e.g., human blood plasma) matters which is vital to reaching the expectation level of drinking water standard (LOD < 10 nM).

Materials and methods

Materials

In the current study, all of the utilized chemical compounds including NH_3, $(NH_4)_2S_2O_8$, HCl, $C_6H_5NH_2$ (i.e., aniline monomer), NH_4OH, $FeCl_3{\cdot}6H_2O$, $FeSO_4{\cdot}7H_2O$, and acetone were provided by Merck & Co. Silver diethyldithiocarbamate (i.e., $(C_2H_5)_2NCSSAg$) was used as the main part of the absorber/sensor toward detection of mercury within aquatic media which was supplied by Fisher Scientific International, Inc. All of the reagents used were selected from high-purity analytical grade and used without further purification expect for aniline monomer that was vacuum-distilled before used. Other utilized materials for experimental evaluations including NaOH, HNO_3, and $HgCl_2$ were supplied by Merck & Co.

Preparation of nanomaterials

Fabrication of magnetite nanoparticles

Fabrication procedure of magnetite nanoparticles (i.e., Fe_3O_4) was conducted based on our previous procedures [45, 54–56]. Briefly, 4.55 g $FeCl_3{\cdot}6H_2O$ and 3.89 g $FeSO_4{\cdot}7H_2O$ were added to 320 mL deionized (DI) water and stirred at 80 °C

for 1 h until obtaining a fully homogeneous suspension. Next, 40 mL ammonia was dropwise added to the suspension and stirred for further 2 h. The synthesized supermagnetic nanoparticles were separated via a strong magnet and washed several times with DI water. The obtained powder was dried in an oven at 100 °C for 2 h and kept in a desiccator until further use.

Synthesis of polyaniline-based structures

Fabrication of PANi was conducted the same as in our previous study [45]; in this matter, first, 9.1 g ammonium persulfate and 3.72 g aniline monomer were separately added to 50 mL 1 M HCl and stirred at room temperature (RT) until becoming fully uniform. Then, aniline solvent was poured in a vessel and cooled down to less than 5 °C using ice bath. Afterward, suspension of ammonium persulfate was dropwise added to the aniline solvent and stirred for 24 h until full polymerization of monomer. The obtained blackish green powder was vacuum-filtrated and thence washed with DI water, 0.2 M HCl, acetone, and DI water, respectively. Finally, the obtained powder was fully dried in an oven at 60 °C for 12 h.

For fabrication of modified polyaniline with silver diethyldithiocarbamate and Fe_3O_4 nanoparticles, 5 wt% silver diethyldithiocarbamate and 5 wt% Fe_3O_4 (with respect to the weight of aniline monomer) were added to 50 mL HCl and ultrasonicated for 30 min at 600 W. Thereafter, the aniline monomer was added to this suspension and the rest of the process was performed according to the aforementioned procedure.

Materials and apparatus for electrochemical evaluations

Ultrapure water was used during the experiment to prepare required solutions. Solution of phosphate buffer (10 mM PBS) as the supporting electrolyte was prepared using mixed stock solutions of K_2HPO_4 and KH_2PO_4 and employed for electrochemical analysis of mercury ions. Standard solutions of Hg^{2+} (i.e., 100.0 mg L^{-1}) were prepared via dissolving sufficient amounts of mercury(II) chloride ($HgCl_2$) in ultrapure water. Various concentrations of mercury ions were obtained by diluting the highly concentrated standard stock solution.

Besides, all of the electrochemical measurements were recorded with GCE (with 5-mm diameter) as the working electrode, platinum wire (Pt, 0.5-mm diameter) as the auxiliary electrode, and commercial Ag/AgCl (saturated with 3 M KCl) as the reference electrode, assembled in a 20-mL three-electrode cell system. An electrochemical setup (Metrohm, Autolab model PGSTAT 302N) was used for analyzing the electrochemical data. The electrochemical impedance spectroscopy (EIS) analysis was conducted through applying 10-mV amplitude AC potential over 220 mV of DC potential from 100-kHz to 1-Hz frequencies within the KCl solution (0.01 M) containing $[Fe(CN)_6]^{3-/4-}$ redox couple.

The Nyquist plots in EIS provide information regarding the nature of impedance data. The R_{ct} value as charge transfer resistance was acquired using Zview simulation software. Cyclic voltammograms (CVs) were gathered in the range of − 1.0 and 1.0 V and scan rate of 100 mV s^{-1} in PBS with pH 7. Differential pulse anodic stripping voltammetry (DPASV) tests were carried out by applying potential ranging from − 0.8 to 0.6 V using 0.01 M PBS (pH 7.0) with 25-mV amplitude, 5-mV step potential, and 120-s deposition time at − 0.8 V.

Fabrication of biosensor

During each test and modification process, the main GCE was well cleaned using alumina slurry with diverse dimensions (i.e., 0.3 and 0.05 μm) and then ultrasonically rinsed with aqueous ethanol for 5.0 min. Thereafter, the GCE was cleaned electrochemically via sweeping CV from − 0.2 to + 1.2 V (vs. Ag/AgCl) at 100 mV s^{-1} in H_2SO_4 solution (0.5 M) to reach the optimum condition. Afterward, the pre-treated electrode was rinsed thoroughly with deionized (DI) water and dried at RT (25.0 ± 0.1 °C). The modified electrodes were obtained by a drop casting method. In this case, the developed nanostructures were dispersed within the ultrapure water (2 mg mL^{-1}) through ultrasonicating for about 30 min to get a homogeneous and stable suspension. Typically, 10 μL of the prepared suspension was dropped onto the prepared surface of the working electrode and allowed to dry in air at RT.

Electrochemical measurements

The analysis of Hg^{2+} ions was performed using DPASV in PBS (pH 7.0) as follows: the pre-concentration step was performed at − 0.8 V vs. Ag/AgCl in the period of 120 s; thence, the differential pulse voltammograms were achieved within the range of − 0.8 V to 0.6 V vs. Ag/AgCl at RT. The calibration plots were prepared via plotting the oxidation peak currents vs. different concentrations of Hg^{2+}, whereas the LOD and LOQ (3 and 10 s/slope ratios, respectively) were calculated by considering the σ as the standard deviation in the mean value which corresponds to 10 replicates of current response on reagent blanks [57]. In addition, the sensor performance for the selectivity of the PANi-F-S-GCE toward detection of Hg^{2+} was surveyed against buffer solution containing different cations as interfering contents (e.g., Cu^{2+}, Pb^{2+}, Zn^{2+}, Co^{2+}, Cd^{2+}, and Ni^{2+}). The detection of Hg^{2+} was repeated 3 times, and the measurements for various metal ions were performed under the same conditions.

Preparation of real samples

Water samples (Vata mineral water, tap water, and industrial wastewater; appropriate permissions were taken from responsible authorities for collecting industrial wastewater toward evaluating the performance of modified electrode) and biological samples (human blood plasma) have been utilized for evaluating the applicability of the developed sensor for tracing mercury ion quantity in real aqua samples. The water samples were placed within a 20-mL tube and passed through a standard filter paper (Whatman No. 40). Human blood plasma as a biological real sample was obtained from Fars Blood Transfusion Center (Shiraz, Fars, Iran) from healthy volunteers. In this case, 1.0 mL of plasma samples was poured into the centrifuge tube thoroughly mixed with H_2SO_4 (0.5 M) followed by centrifugation at 3500 rpm for 15 min to separate unwanted proteins. Afterward, the supernatant solution was 5 times diluted with ultrapure water and adjusted to pH 7.0. The reliability of the described method was verified by the analysis of water and human plasma samples spiked with known amounts of Hg^{2+} and estimation was carried out by considering the recovery rate as the criterion.

Results and discussions

Characterization of developed nanomaterials

In this section, developed nanomaterials were subjected to diverse analyses in order to validate their successful fabrication. In Fig. 1a, the FTIR spectrum of Fe_3O_4 nanoparticles (NPs) can be seen. In this regard, each appearing peak corresponds to stretching vibration of Fe–O (579 cm^{-1}), C–H (929 cm^{-1}), $FeOO^-$ (1622 cm^{-1}), C–H (2921 cm^{-1}), and –OH (3430 cm^{-1}) functional groups. Appearance of these peaks along with existence of Fe_3O_4 fingerprint at 579 and 1622 cm^{-1} clearly confirmed the successful fabrication of Fe_3O_4 nanoparticles [45]. In Fig. 1b, the X-ray diffractogram of Fe_3O_4 NPs can be seen. As shown in this figure, each appearing diffraction peak corresponds to (peak 2 /plane) 18.5/(111), 30.18/(220), 35.75/(311), 43.30/(400), 53.88/(422), 57.19/(511), 62.65/(440), and 74.11/(533) which is in accord with pure spinal magnetite nanoparticles with card number 89-3854 [54, 58, 59].

In Fig. 1c, outcome of vibrating-sample magnetometer (VSM) analysis for the developed magnetite nanoparticles can be seen. As shown, the developed supermagnetic nanoparticles exhibiting an S-like curve with superior magnetization (M_s) of about 69.2 emu g^{-1} demonstrated excellent magnetic properties of the developed nanomaterials. What is more, in Fig. 1d, e, TEM image and size distribution range of the developed nanomaterials can be seen. As depicted in these images, Fe_3O_4 NPs were synthesized with well-defined spherical morphology with size distribution ranging from 7.6 to 22.5 nm, while most of the nanoparticles exhibited size within ranges 10–11.4 nm and 13.1–15 nm. These data along with obtained data from FTIR, XRD, and VSM analyses clearly confirmed the successful fabrication of magnetite nanoparticles with ideal specifications.

In addition, Fig. 2 depicts the FTIR and XRD spectra of polyaniline (PANi) and modified polyaniline with Fe_3O_4 nanoparticles and silver diethyldithiocarbamate (PANi-F-S). As illustrated within part (a), both PANi and PANi-F-S present similar FTIR spectra with some shifts that are due to the interaction of added materials together. In this matter, peaks around wavelength of 785 cm^{-1} are attributed to the vibration of C–H groups within the benzene ring [60]. Appearing peaks within ranges 868–1059 cm^{-1} and 1112–1158 cm^{-1} are attributed to the –NH and vibration of C–H group related to N=quinoid ring (Q)=N, and B–N^+H–B bonds that reveal the presence of charge carriers in the polymeric structure of PANi owing to the superior protonation process. These charge carriers lead to generation of delocalized electrons which improve the electrical conductivity of polyaniline [61, 62]. Additionally, peaks within ranges 1220–1222 cm^{-1} and 1282–1283 cm^{-1} correspond to the C–N^+ and C–N functional groups related to the polaronic structure and stretch of the secondary aromatic amine groups within the structure of polyaniline, respectively.

Furthermore, appearing peaks within ranges 1431–1487 cm^{-1} and 1550–1578 cm^{-1} correspond to the stretching vibration of NH–benzenoid ring (B)–NH and N=quinoid ring (Q)=N, respectively [63, 64]. More importantly, shift of FTIR peaks within FTIR spectrum of PANi-F-S, especially for peaks around 1112 and 1158 cm^{-1}, shows higher degree of protonation in PANi-F-S than pristine PANi. Other peaks between ranges 1900–1903 cm^{-1} and 2091–2093 cm^{-1} are attributed to the C=C double bond carbon atoms [65] and azide functional groups (i.e., $N^- \equiv N^+ = N^-$) [66], respectively. Large shoulder in the FTIR spectrum of PANi-F-S of about 3212 cm^{-1} corresponds to hydroxyl functional groups (i.e., –OH) [67].

In Fig. 2b, the XRD spectrum of PANi can be seen. As illustrated, 2 peaks at 14.9, 20.7, and 25.2 are attributed to the (112), (020), and (200) crystal planes of polyaniline, respectively. These data along with obtained data from FTIR analyses clearly confirmed the successful fabrication of our PANi of primary monomer [67–69]. On the other hand, PANi-F-S showed a highly crystalline structure upon its interaction with Fe_3O_4 NPs and silver diethyldithiocarbamate (Fig. 3c). In this matter, PANi-F-S showed 98 well-defined diffraction peaks that correspond to the presence of highly interconnected compounds of Ag_8S_4, Ag_2S, Ag_2O_3, Ag_3O_4, Ag_4O_4, AgO, $Fe_{24}O_{32}$, $Fe_{28}S_{32}$, $Fe_{16}O_{20}$, $Fe_{24}O_{24}$, $Fe_{12}C_4$, H_4, C_4, $C_4H_{16}N_{24}$, $C_{20}H_{24}N_8O_{16}$, $C_{18}H_{20}N_4O_8$, $C_{16}H_{24}N_8O_8$, $C_4H_{20}N_4O_8$, $C_{24}H_{24}$, and N_2S_2 [45].

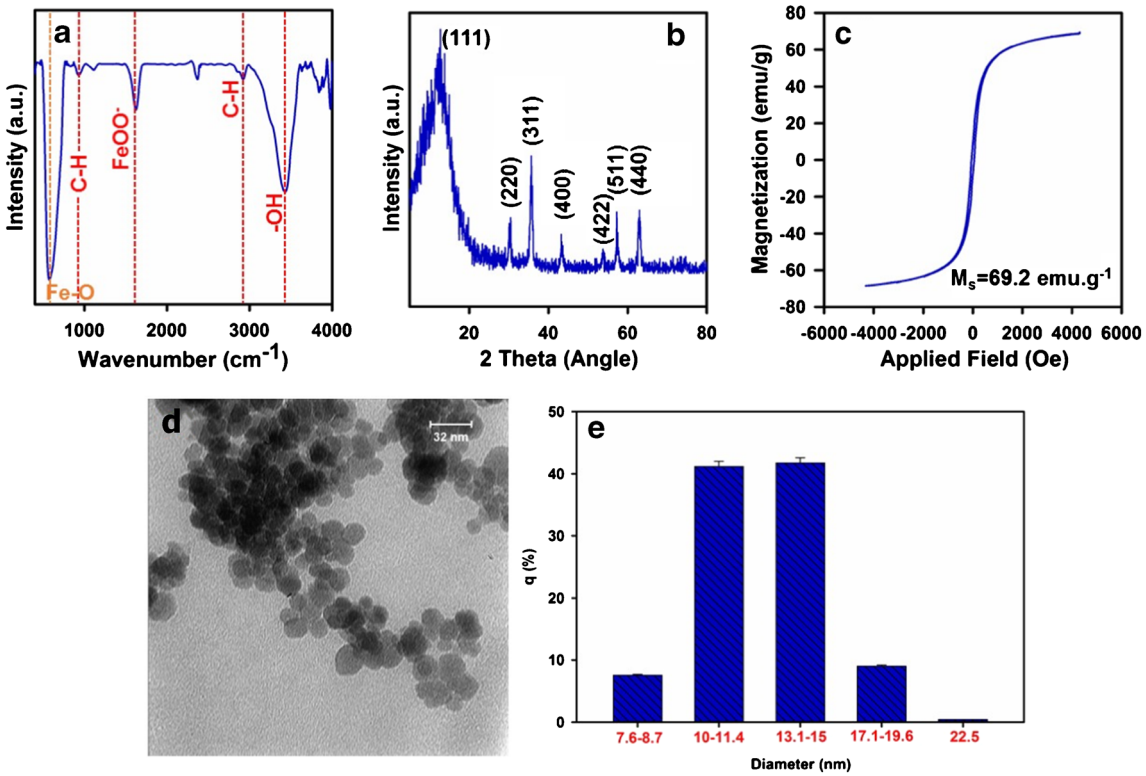

Fig. 1 **a** FTIR spectrum, **b** X-ray diffractogram, **c** VSM analysis, **d** TEM image, and **e** size distribution report (i.e., PSA) of Fe_3O_4 nanoparticles

Fig. 2 **a** FTIR spectrum of PANi and PANi-F-S. **b** XRD spectrum of PANi. **c** XRD spectrum PANi-F-S

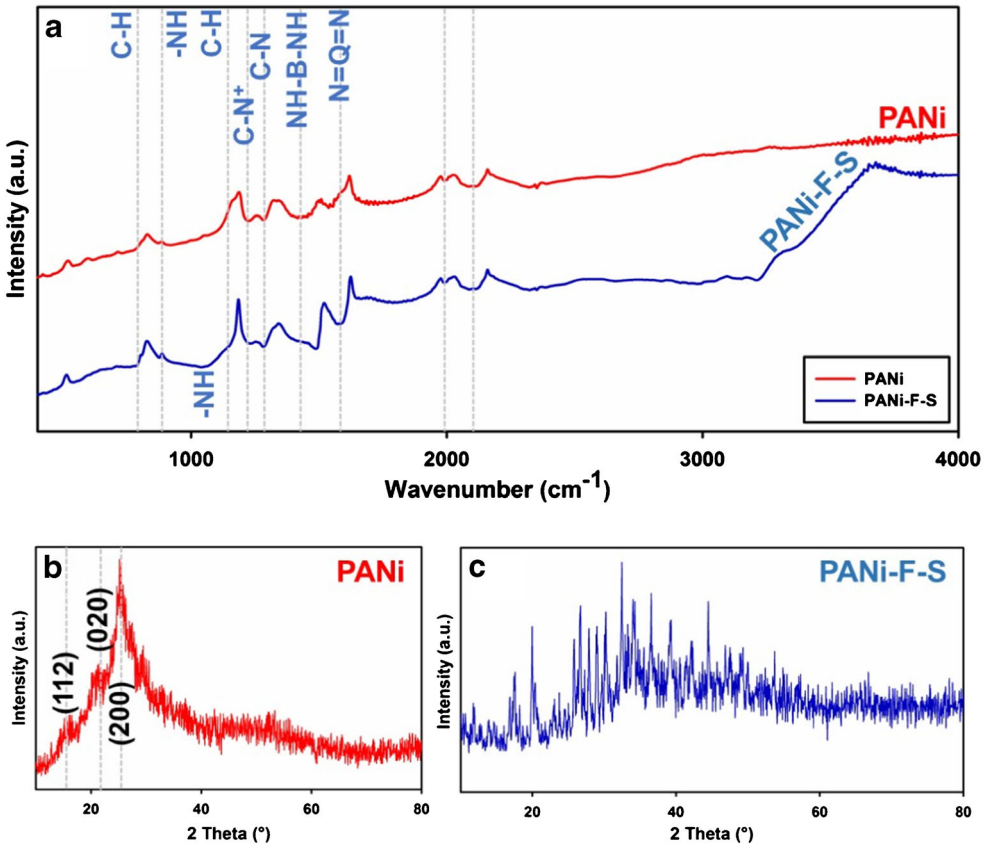

In Fig. 3, FESEM images of PANi and PANi-F-S can be seen at different scale bars (i.e., 10 μm, 2 μm, and 200 nm). As illustrated within Fig. 3a–c, PANi exhibited a tube-shaped structure with nearly uniform size distribution. Addition of silver diethyldithiocarbamate along with magnetite nanoparticles significantly changed the morphology of PANi from tube-shaped to nearly cubic structure with a variable size. In Fig. 3d–f, a view of these images at different scale bars can be seen.

Electrochemical evaluation of the developed sensor

The cyclic voltammograms were recorded at unmodified GCE and modified electrode with a developed nanocomposite (i.e., PANi-F-S) within a solution containing 0.1 M KCl and 1.0 mM of $[Fe(CN)_6]^{3-/4-}$ redox to compare the performance of the developed electrodes (Fig. 4a). The modified GCE has notably higher i_{pa} value compared with the unmodified GCE, representing faster electron transfer rate and enhanced electrocatalytic behavior for the modified electrode upon its surface modification with PANi-F-S. The concentration of the PANi-F-S on the surface of the electrode can be estimated based on the Brown-Anson model which is as follows [70]:

$$I_P = n^2 F^2 I^* AV/4RT \quad (1)$$

where F and n are the Faraday constant (96,485 C mol^{-1}) and number of transferred electrons, respectively, while I^* represents the concentration on the surface of the electrode (mol cm^{-2}). Additionally, parameters A, R, V, and T are attributed to the surface area of GCE (0.5 cm^2), scan rate (100 mV s^{-1}), gas constant (8.314 J mol^{-1} K^{-1}), and temperature (298 K). The value of the surface concentration of the modified GCE measured to be 2.93×10^{-9} mol cm^{-2}.

In addition, the characterization of the fabricated electrochemical sensor/biosensor was traced through the EIS method (see Electronic Supplementary Material (ESM) Fig. S1 (a)). The charge transfer process of the modified GCE was verified by calculating the R_{ct} value as the charge transfer resistance at the interface of the electrode and electrolyte. The Nyquist graphs consisted of linear portion at lower frequency and a semicircle part at higher frequency range indicating a diffusion and limited electron transfer process, respectively. Additionally, the impedance data are in good accordance with the obtained results from CV scans and clearly confirmed the superior role of PANi-F-S for enhancing the electron transfer rate at the surface of the enhanced electrode. Related curves of modified GCE with PANi-F-S exhibited obviously smaller R_{ct} values compared with unmodified GCE, showing that the presence of the PANi-F-S nanocomposite on the surface of the enhanced electrode can significantly improve the electron transfer process.

To further highlight the effect of deposited nanocomposites on the GCE surface toward sensing Hg ions within the aqua solution, the electrochemical measurements of PANi-F-S-modified electrodes were carried out by EIS and CV.

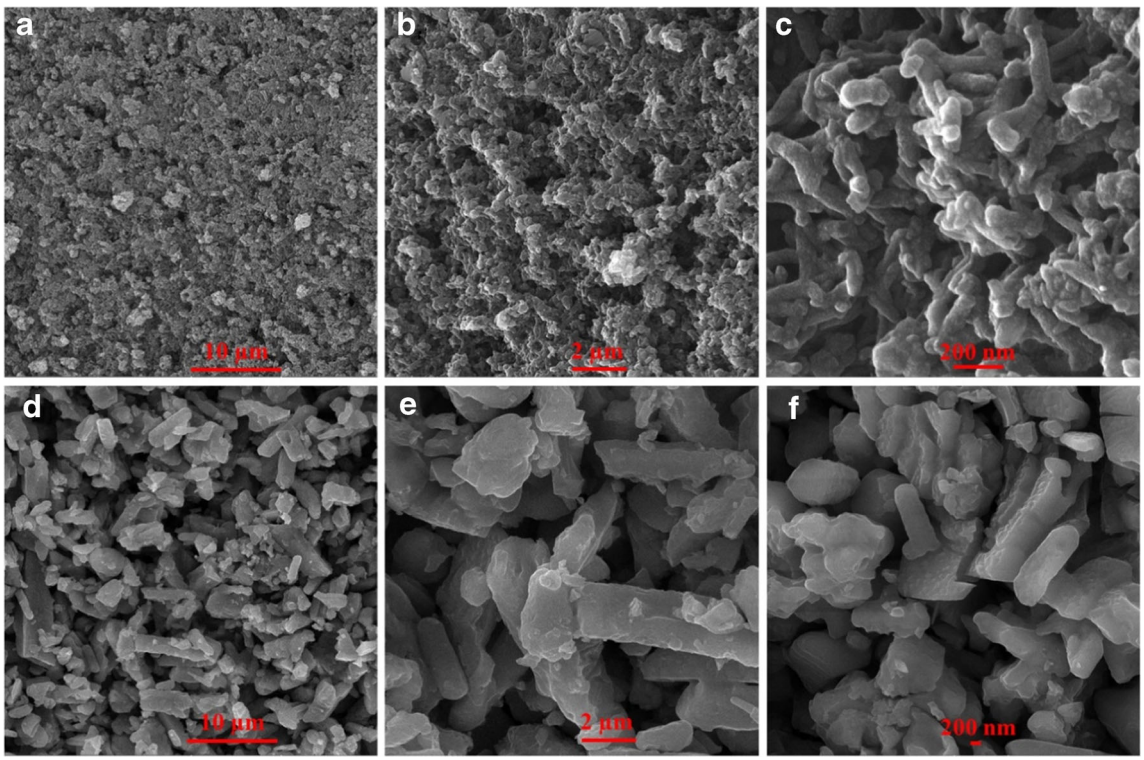

Fig. 3 FESEM images of PANi (**a**–**c**) and PANi-F-S (**d**–**f**) at 10-μm, 2-μm, and 200-nm scale bars

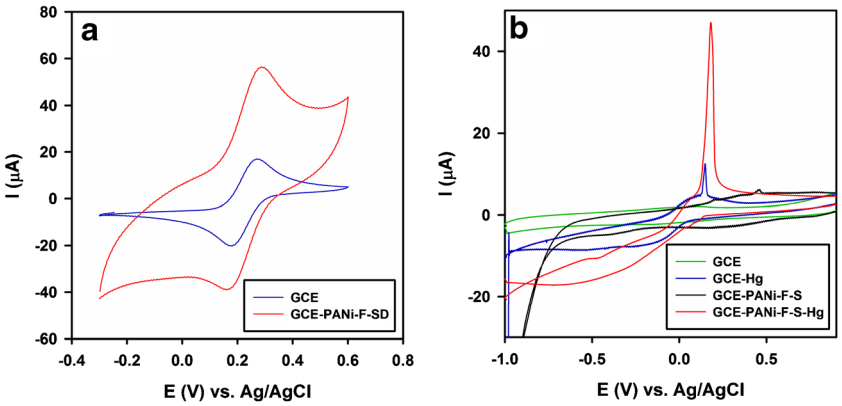

Fig. 4 **a** CV for GCE and GCE-PANi-F-S electrodes in 1.0 mM of $[Fe(CN)_6]^{3-/4-}$. **b** CV plots recorded by different electrodes containing 0.05 μM Hg^{2+}

Figure 4b shows the cyclic voltammetric behavior of mercury (Hg^{2+}) added to PBS (0.01 M, pH 7.0) containing 0.04 μM $HgCl_2$ solution at the bare GCE and modified GCE with the scan rate of 100 mV s^{-1}. As depicted in Fig. 4b, no significant electrochemical responses are recorded at unmodified GCE. Moreover, owing to the ability of the forming complex between Hg^{2+} and S on the electrode surface, a well-defined oxidative current appeared at about 0.17 V vs. Ag/AgCl for Hg^{2+}. This behavior on the modified electrode surface corresponded to the electrochemical oxidation of metallic mercury ($Hg^0 \rightarrow Hg^{2+} + 2e^-$) and indicated that the exposed surface of S can effectively sense Hg^{2+} ions within the aqueous media. The captured Hg^{2+} ions via the PANi-F-S-modified electrode lead to the formation of specific S–Hg^{2+}–S bonds, where the electrochemical response (peak currents) was detected at about 0.17 V. The EIS data are in well accord with the CV results (ESM Fig. S1 (b)). The EIS data demonstrated that the R_{ct} (12 kΩ) values become higher by appearance of Hg^{2+} ions' oxidation peak.

In the case of declaring the mechanism for capturing/sensing the Hg^{2+} ions on PANi-F-S-modified electrodes, the obtained maximum response for Hg^{2+} can be expressed on the basis of Pearson's theory, which indicates that hard/hard acids tend to coordinate with hard/soft bases [71]. Therefore, interactions of Hg^{2+} ions within a solution with functional groups on the surface of the developed nanocomposites are favored. In addition, enhancement of the GCE with PANi-F-S nanocomposite improved the electrochemical currents of Hg^{2+} ions owing to its conductive features. To obtain the optimum experimental conditions, effective parameters in the proposed process including pH and type of supporting electrolyte as well as deposition potential and deposition time for 0.04 μM of Hg^{2+} were evaluated.

Mercury (Hg^{2+}) ions show different electrochemical responses in diverse supporting electrolytes. Therefore, the effect of each electrolyte nature with variable pH values on the peak current response of the developed GCE was investigated. In this case, the effect of electrolytes including 0.1 M HCl, 0.5 M H_2SO_4, 0.1 M KCl, and 0.01 M PBS on the oxidation peak currents of Hg^{2+} showed that the Hg^{2+} ions exhibit the best electrochemical responses with the lowest background in the 0.01 M PBS as the supporting electrolyte.

The value of pH in buffer solution is a significant parameter that highly affects the electrochemical responses of Hg^{2+} ions and the sensitivity of the developed sensor/biosensor [72]. The influence of pH on the oxidation peak current of Hg^{2+} at PANi-F-S-modified electrode was investigated in 0.01 M PBS containing 0.04 μM Hg^{2+} ions (Fig. 5a). As can be seen in Fig. 5a, the peak current increased in the pH value ranging from 3 to 7 and then decreased at pH value of 8. The reason for this process could be attributed to the precipitation of Hg^{2+} at higher pH values. Therefore, pH 7 is considered as the optimum pH value for the subsequent electrochemical experiments.

Deposition potential is another main parameter on the mercury stripping peak currents which should be considered during evaluations. In this regard, accumulation of 0.04 μM of Hg^{2+} was verified on the surface of PANi-F-S-GCE from − 0.4 to − 1.0 V vs. Ag/AgCl with the deposition time of 120 s. As illustrated in Fig. 5b, by further shifting the potential from − 0.4 to − 1.0 V vs. Ag/AgCl, the stripping voltammetric signals considerably enhanced. As the accumulation potential trends to more negative values, the current signals for Hg^{2+} were weakened due to the considerable effect of hydrogen evolution in this media, while the deposited metals on the surface of the electrode can be affected via hydrogen bubbles. Therefore, − 0.8 V was chosen for the subsequent tests owing to its ideal sensitivity and well-defined oxidation peaks.

The influence of the deposition time on the stripping current signal was also investigated within the range of 30 to 180 s. Figure 5c illustrated that by prolonging the deposition time, the stripping oxidation current of Hg^{2+} and its sensing became far better. By further increasing the accumulation time, current was leveled off and reached the constant situation. However, the saturation adsorption of active sites on the electrode surface was achieved after 120 s preconcentration. Thereafter, further prolonging the deposition time has no significant effect on the signal enhancement rate. Thereby, the

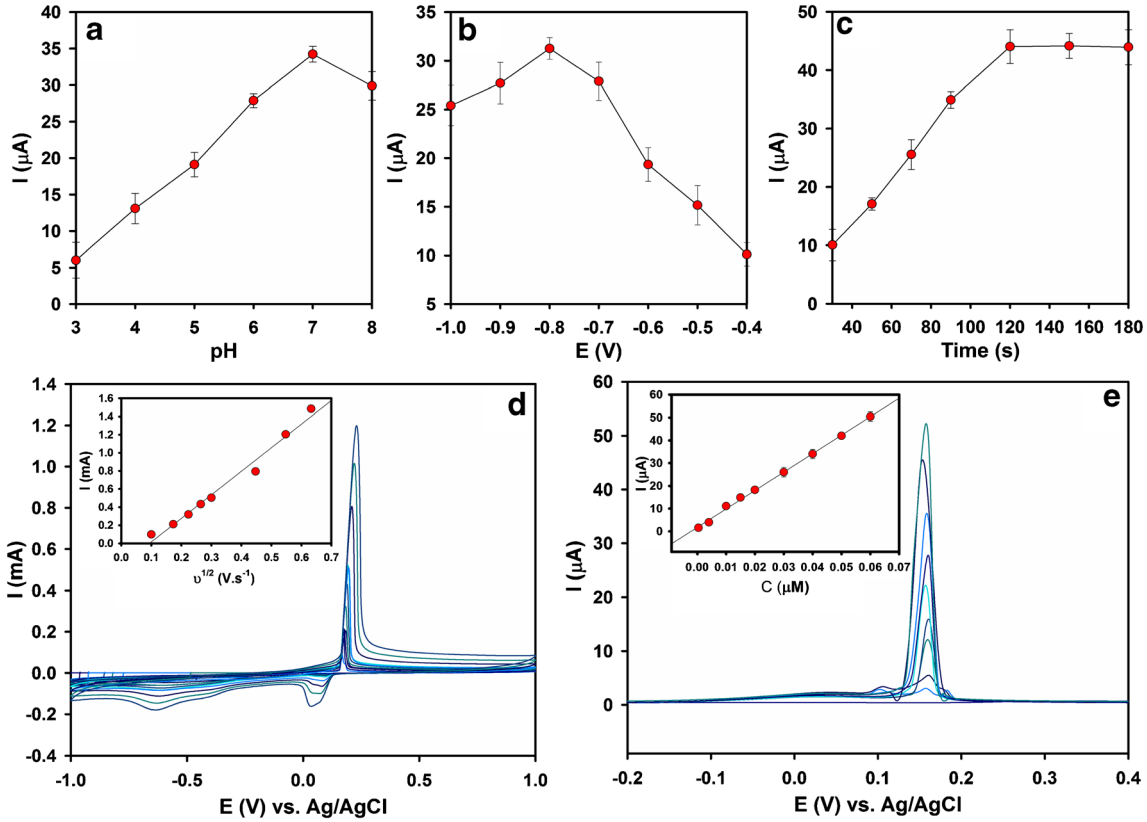

Fig. 5 Effect of pH (**a**), accumulation potential (**b**), and deposition time (**c**) on the current responses of 0.05 μM Hg^{2+} on GCE-PANi-F-S electrode. Error bar indicates the standard deviation of three replicate measurements, CV (**d**) recorded at different scan rates from 0.01 to 0.4 V s^{-1} in 0.01 mol L^{-1} PBS (pH 7.0), and DPV curves (**e**) of different concentrations of Hg^{2+} captured by PANi-F-S-modified electrode at optimal conditions: pH 7.0, accumulation potential of − 0.8 V, deposition time of 120 s, modulation amplitude of 25 mV, and step potential of 5 mV. Inset shows the obtained calibration curve for the modified electrode

accumulation time of 120 s was chosen as the optimum condition for the following experiments.

The kinetic of the modified GCE with PANi-F-S was investigated under different scan rates from 10 to 400 mV s^{-1} (Fig. 5d). In this matter, the electrochemical oxidation signal has a linear relationship with the square root of the scan rate which indicated that the nature of electrochemical process is governed through the diffusion process.

DPV as one of the most sensitive electrochemical methods is used for the detection of analytes owing to its high sensitivity and low detection limit. The DPV graphs for diverse concentrations of mercury ions are depicted in Fig. 5e. The modified GCE exhibited a sensitive response to various concentrations of Hg^{2+} and showed an increasing trend in the oxidation signal upon addition of mercury ions. Furthermore, the current signal of voltammograms increased proportionally upon increase in the concentration of Hg ions in the range of 0.4–60 nM, while the calibration curve showed a linear current increase by further increasing the overall amount of Hg^{2+} ions (I (μA) = 809.43 C(μM) + 1.8174).

The linear relative coefficient, limit of detection, and limit of quantification were calculated to be 0.9983, 0.051 nM, and 0.14 nM, respectively, demonstrating significantly high sensitivity of the modified GCE until picomolar level which is ideal for precise detection of Hg^{2+} within non-biological/biological aqueous media. Moreover, the modified GCE with PANi-F-S demonstrated a remarkably high sensitivity of about 1618.86 μA $μM^{-1}$ cm^{-2} by dividing the slope of the calibration curve to the geometric surface area of the electrode (0.5 cm^2) [73]. This significantly high sensitivity could be due to the strong affinity of Hg^{2+} and deposited nanocomposite on the surface of electrode along with the electrochemical response amplified by the conductive nature of polyaniline. The obtained results clearly confirmed the superior sensitivity of the modified GCE toward detection of Hg^{2+} within aqueous media.

To further evaluate the reproducibility of the proposed method, two different PANi-F-S-modified electrodes were tested in completely identical conditions toward detection of 0.04 μM Hg^{2+} in 0.01 M PBS. The DPV responses exhibited a relative standard deviation (RSD) of 3.66% for mercury, confirming that the sensor is reproducible. The intra-/inter-day reliability was also estimated by performing 10 times determination of the same sample containing 0.04 μM Hg^{2+} in 1 day and in 5 days, where the RSD value for repetitive stripping voltammograms on the same modified electrode was

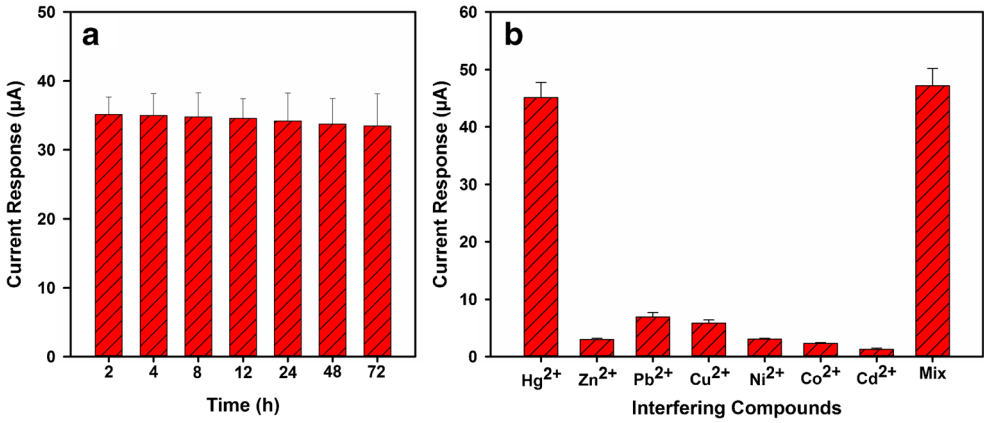

Fig. 6 **a** Stability response of the modified electrode with PANi-F-S. **b** Current responses of modified electrode with PANi-F-S to different metal ions in PBS pH (7.0). Error bars correspond to the standard deviation of three replicate tests

found to be about 2.56% and 4.12%, respectively. In case of evaluating the stability of modified GCE, the DPV currents for 0.04 μM Hg^{2+} in 0.01 M PBS (pH 7.0) were recorded over a period of 72 h. In this matter, based on our results, the oxidation current was not significantly changed and has nearly the same value with a RSD of 4.67% (Fig. 6a). These obtained data clearly showed that the modification of GCE with PANi-F-S can considerably improve the stability and reproducibility of the modified electrode toward accurate determination of Hg^{2+} ions within aqueous media.

The developed biosensor's selectivity toward detection of Hg^{2+} (0.05 μM) was verified in the presence of common interfering heavy metal ions including Pb^{2+}, Zn^{2+}, Ni^{2+}, Co^{2+}, Cd^{2+}, and Cu^{2+} with tenfold concentration of Hg^{2+}, and metal interference was examined by investigating the influence of other metals on the stripping signal. The outcome of electrochemical responses displayed that the value of the modified electrode in the presence of Hg^{2+} is greater than that in the presence of other metal ions (Fig. 6b). The stripping peak current of Hg^{2+} changes slightly in the mixing sample, indicating that these metal ions do not interfere with the determination of Hg^{2+}. From these evaluations, it can be found that the high selectivity of the sensing method is due to the specific coordination between catalyst and Hg ions. The electrode has strong affinity toward Hg^{2+} ions and bind selectively to S deposited on the modified surface and form stable S-Hg^{2+}-S complexes.

To study the reusability of the PANi-F-S electrode, the electrode was soaked in 500 mM EDTA solution for about 1 h after each measurement. As depicted in ESM Fig. S2, the modified electrode with PANi-F-S showed a slight decrease in the current signal (about 5%) compared with the primary scan. Besides, further investigation showed that after about 10 cycles of regeneration process, the recovered electrode could retain about 89% of its optimum/primary current signal which exhibits the potential of developed electrode to be reused for subsequent detection of Hg^{2+} ions within aquatic media.

The applicability of the PANi-F-S-modified electrode was assessed in different water and biological samples according to Eq. 2. Three various concentrations of Hg^{2+} were spiked to each of the real samples where the related outcomes can be seen within Table 3. As tabulated in Table 3, the obtained recovery percentages more than 92% confirmed that the developed PANi-F-S-GCE equipped with ideal features for precise determination of Hg^{2+} ions within non-biological/biological aquatic environments (e.g., water samples and human blood plasma sample) makes it an ideal multi-functional platform for accurate detection of Hg^{2+} within diverse media.

$$\text{Recovery}\ (\%) = \frac{C_{\text{found}} - C_{\text{real}}}{C_{\text{spiked}}} \times 100 \qquad (2)$$

Conclusions

Distribution of superiorly toxic heavy metals such as mercury within the ecosystem can adversely affect the life of living species and top consumers in the food chain via bioaccumulation within food sources. Therefore, it is bare bone essential

Table 3 Recoveries and RSD of spiked Hg^{2+} in different samples

Samples	Spiked (μM)	Found (μM)	Recovery* (RSD) %
Mineral water	0.005	0.00506	101.2 ± 4.43
	0.01	0.0092	92.0 ± 1.98
	0.06	0.0596	99.33 ± 5.12
Tap water	0.005	0.0047	94.0 ± 5.06
	0.01	0.0097	97.0 ± 4.12
	0.06	0.0602	100.3 ± 2.48
Industrial wastewater	0.005	0.0109	101.4 ± 3.23
	0.01	0.0155	96.7 ± 2.05
	0.06	0.0612	92.2 ± 3.87
Plasma	0.005	0.00503	100.6 ± 3.12
	0.01	0.0104	104.0 ± 4.37
	0.06	0.0595	99.16 ± 4.05

to develop highly accurate sensors/biosensors for detection of mercury in ranges less than 10 nM. In this matter, the modified GCE with PANi-F-S electrode proved to be a highly sensitive and accurate sensor for detection of Hg^{2+} ions within non-biological and biological aqueous media. In this matter, obtained data from electrochemical evaluations showed that the modified GCE exhibiting LOD and sensitivity of 0.01 nM and 1618.86 mA mM^{-1} cm^{-2}, respectively, at optimum sensing conditions confirms the ideal capability of the developed electrode for accurate detection of Hg^{2+} ions until picomolar level. Moreover, the modified GCE also showed fantastic repeatability, stability, reproducibility, and selectivity and exhibited recovery ranges more than 99% for detection of Hg^{2+} ions within non-biological and biological aqueous media.

Compliance with ethical standards The studies have been performed in accordance with the ethical standards and approved through following the protocols of the ethical committee. The human blood plasma sample is provided from the stock of Fars Blood Transfusion Center (Shiraz, Fars, Iran) that was obtained from a healthy volunteer with full consent of donor. The reference and LOT of the supplied human blood plasma sample are MDE650Q and 11275071CM, respectively.

Conflict of interest The authors declare that they have no conflict of interest.

References

1. Gumpu MB, Sethuraman S, Krishnan UM, Rayappan JBB. A review on detection of heavy metal ions in water–an electrochemical approach. Sensors Actuators B Chem. 2015;213:515–33.
2. Ray PD, Yosim A, Fry RC. Incorporating epigenetic data into the risk assessment process for the toxic metals arsenic, cadmium, chromium, lead, and mercury: strategies and challenges. Front Genet. 2014;5:201.
3. ATSDR T ATSDR (Agency for Toxic Substances and Disease Registry). Prepared by Clement International Corp, under contract 205:88-0608.
4. Carocci A, Rovito N, Sinicropi MS, Genchi G. Mercury toxicity and neurodegenerative effects. In: Reviews of environmental contamination and toxicology: Springer. 2014;229:1–18.
5. Zhang Y, Zeng GM, Tang L, Chen J, Zhu Y, He XX, et al. Electrochemical sensor based on electrodeposited graphene-Au modified electrode and nanoAu carrier amplified signal strategy for attomolar mercury detection. Anal Chem. 2015;87(2):989–96.
6. Kidd K, Clayden M, Jardine T. Bioaccumulation and biomagnification of mercury through food webs. Hoboken: Environmental chemistry and toxicology of mercury Wiley; 2012. p. 455–99.
7. Chen G, Guo Z, Zeng G, Tang L. Fluorescent and colorimetric sensors for environmental mercury detection. Analyst. 2015;140(16):5400–43.
8. Hu J, Li J, Qi J, Chen J. Highly selective and effective mercury (II) fluorescent sensors. New J Chem. 2015;39(2):843–8.
9. Mandal P, Debbarma S, Saha A, Ruj B. Disposal problem of arsenic sludge generated during arsenic removal from drinking water. Procedia Environ Sci. 2016;35:943–9.
10. Li Y, Wang J, Luan Z, Liang Z. Arsenic removal from aqueous solution using ferrous based red mud sludge. J Hazard Mater. 2010;177(1–3):131–7.
11. Clarke ML, Harvey DG, Humphreys DJ.Veterinary toxicology. vol 2nd edition. London: Bailliere Tindall. 1981.
12. Bressler JP, Goldstein GW. Mechanisms of lead neurotoxicity. Biochem Pharmacol. 1991;41(4):479–84.
13. Rossi E. Low level environmental lead exposure–a continuing challenge. Clin Biochem Rev. 2008;29(2):63.
14. Ghosh A, Sen S, Sharma A, Talukder G. Effect of chlorophyllin on mercuric chloride-induced clastogenicity in mice. Food Chem Toxicol. 1991;29(11):777–9.
15. Solecki R, Hothorn L, Holzweissig M, Heinrich V. Computerised analysis of pathological findings in longterm trials with phenylmercuric acetate in rats. In: Recent developments in toxicology: trends, methods and problems: Springer. 1991;4:100–3.
16. Thuvander A, Sundberg J, Oskarsson A. Immunomodulating effects after perinatal exposure to methylmercury in mice. Toxicology. 1996;114(2):163–75.
17. Clarkson TW. Metal toxicity in the central nervous system. Environ Health Perspect. 1987;75:59–64.
18. Wright RO, Baccarelli A. Metals and neurotoxicology. J Nutr. 2007;137(12):2809–13.
19. Almeida P, Stearns LB. Political opportunities and local grassroots environmental movements: the case of Minamata. Soc Probl. 1998;45(1):37–60.
20. Hartwig A. Cadmium and cancer. In: Cadmium: from toxicity to essentiality: Springer. 2013;11:491–507.
21. Salnikow K, Zhitkovich A. Genetic and epigenetic mechanisms in metal carcinogenesis and cocarcinogenesis: nickel, arsenic, and chromium. Chem Res Toxicol. 2007;21(1):28–44.
22. Jeong ED, Won MS, Shim YB. Simultaneous determination of lead, copper, and mercury at a modified carbon paste eletrode containing humic acid. Electroanalysis. 1994;6(10):887–93.
23. Ugo P, Moretto LM, Mazzocchin GA. Voltammetric determination of trace mercury in chloride media at glassy carbon electrodes modified with polycationic ionomers. Anal Chim Acta. 1995;305(1–3):74–82.
24. Ugo P, Sperni L, Moretto LM. Ion-exchange voltammetry of trace mercury (II) at glassy carbon electrodes coated with a cationic polypyrrole derivative. Application to pore-waters analysis. Electroanalysis. 1997;9(15):1153–8.
25. Sharma SK, Kaur N, Singh J, Singh A, Raj P, Sankar S, et al. Salen decorated nanostructured ZnO chemosensor for the detection of mercuric ions (Hg2+). Sensors Actuators B Chem. 2016;232:712–21.
26. Li W, Li Y, Qian H-L, Zhao X, Yang C-X, Yan X-P. Fabrication of a covalent organic framework and its gold nanoparticle hybrids as stable mimetic peroxidase for sensitive and selective colorimetric detection of mercury in water samples. Talanta. 2019;204:224–8.
27. Mubarok AZ, Lin S-T, Mani V, Huang C-H, Huang S-T. Design of controlled multi-probe coupled assay via bioinspired signal amplification approach for mercury detection. RSC Adv. 2016;6(63):58485–92.
28. Jeromiyas N, Elaiyappillai E, Kumar AS, Huang S-T, Mani V. Bismuth nanoparticles decorated graphenated carbon nanotubes modified screen-printed electrode for mercury detection. J Taiwan Inst Chem Eng. 2019;95:466–74.
29. Manavalan S, Govindasamy M, Chen S-M, Rajaji U, Chen T-W, Ali MA, et al. Reduced graphene oxide supported raspberry-like SrWO4 for sensitive detection of catechol in green tea and drinking water samples. J Taiwan Inst Chem Eng. 2018;89:215–23.
30. Govindasamy M, Manavalan S, Chen S-M, Rajaji U, Chen T-W, Al-Hemaid FM, et al. Determination of neurotransmitter in biological and drug samples using gold nanorods decorated f-MWCNTs modified electrode. J Electrochem Soc. 2018;165(9):B370–7.

31. Govindasamy M, Rajaji U, Chen S-M, Kumaravel S, Chen T-W, Al-Hemaid FM, et al. Detection of pesticide residues (Fenitrothion) in fruit samples based on niobium carbide@ molybdenum nanocomposite: an electrocatalytic approach. Anal Chim Acta. 2018;1030:52–60.
32. Sharma VV, Tonelli D, Guadagnini L, Gazzano M. Copper-cobalt hexacyanoferrate modified glassy carbon electrode for an indirect electrochemical determination of mercury. Sensors Actuators B Chem. 2017;238:9–15.
33. Veerakumar P, Veeramani V, Chen S-M, Madhu R, Liu S-B. Palladium nanoparticle incorporated porous activated carbon: electrochemical detection of toxic metal ions. ACS Appl Mater Interfaces. 2016;8(2):1319–26.
34. Sakthinathan S, Tamizhdurai P, Ramesh A, Chiu T-W, Mangesh V, Veerarajan S, et al. Platinum incorporated mordenite zeolite modified glassy carbon electrode used for selective electrochemical detection of mercury ions. Microporous Mesoporous Mater. 2020;292:109770.
35. Shah A, Sultan S, Zahid A, Aftab S, Nisar J, Nayab S, et al. Highly sensitive and selective electrochemical sensor for the trace level detection of mercury and cadmium. Electrochim Acta. 2017;258:1397–403.
36. Rajabi HR, Roushani M, Shamsipur M. Development of a highly selective voltammetric sensor for nanomolar detection of mercury ions using glassy carbon electrode modified with a novel ion imprinted polymeric nanobeads and multi-wall carbon nanotubes. J Electroanal Chem. 2013;693:16–22.
37. Zhang P, Dong S, Gu G, Huang T. Simultaneous determination of Cd 2+, Pb 2+, Cu 2+ and Hg 2+ at a carbon paste electrode modified with ionic liquid-functionalized ordered mesoporous silica. Bull Kor Chem Soc. 2010;31(10):2949–54.
38. Jayadevimanoranjitham J, Narayanan SS. 2, 4, 6-Trimercaptotriazine incorporated gold nanoparticle modified electrode for anodic stripping voltammetric determination of Hg (II). Appl Surf Sci. 2018;448:444–54.
39. Zhou L, Xiong W, Liu S. Preparation of a gold electrode modified with Au–TiO 2 nanoparticles as an electrochemical sensor for the detection of mercury (II) ions. J Mater Sci. 2015;50(2):769–76.
40. Xing H, Xu J, Zhu X, Duan X, Lu L, Wang W, et al. Highly sensitive simultaneous determination of cadmium (II), lead (II), copper (II), and mercury (II) ions on N-doped graphene modified electrode. J Electroanal Chem. 2016;760:52–8.
41. Ordeig O, Banks CE, del Campo J, Muñoz FX, Compton RG. Trace detection of mercury (II) using gold ultra-microelectrode arrays. Electroanalysis Int J Devoted Fundam Pract Aspects Electroanalysis. 2006;18(6):573–8.
42. Sánchez-Calvo A, Fernández-Abedul MT, Blanco-López MC, Costa-García A. Based electrochemical transducer modified with nanomaterials for mercury determination in environmental waters. Sens Actuators B. 2019;290:87–92.
43. Augelli MA, Abarza Munoz RA, Richter EM, Gouveia Junior A, Angnes L. Chronopotentiometric stripping analysis using gold electrodes, an efficient technique for mercury quantification in natural waters. Electroanalysis Int J Devoted Fundam Pract Aspects Electroanalysis. 2005;17(9):755–61.
44. Shah A, Nisar A, Khan K, Nisar J, Niaz A, Ashiq MN, et al. Amino acid functionalized glassy carbon electrode for the simultaneous detection of thallium and mercuric ions. Electrochim Acta. 2019;321:134658.
45. Hashemi SA, Mousavi SM, Ramakrishna S. Effective removal of mercury, arsenic and lead from aqueous media using polyaniline-Fe3O4-silver diethyldithiocarbamate nanostructures. J Clean Prod. 2019;239:118023.
46. Van Erkelens P. Radiometric trace analysis of lead with diethyldithiocarbamate and 204T1. Anal Chim Acta. 1962;26:32–45.
47. Bobtelsky MM, Rafailoff R. A heterometric micro-determination of lead with sodium diethyldithiocarbamate. Anal Chim Acta. 1957;16:321–6.
48. Bobtelsky MM, Rafailoff R. Micro-heterometric determination of bismuth with sodium diethyldithiocarbamate. Anal Chim Acta. 1957;16:488–92.
49. Merry RH, Zarcinas B. Spectrophotometric determination of arsenic and antimony by the silver diethyldithiocarbamate method. Analyst. 1980;105(1251):558–63.
50. Alvarez-Coque MG, Camañas RV, Vaya MM, Ramos GR, Fernandez CM. Spectrophotometric determination of mercury (II) and silver (I) with copper (II) and diethyldithiocarbamate in the presence of triton X-100. Talanta. 1986;33(8):697–9.
51. Bobtelsky M, Rafailoff R. A precise, direct, heterometric microdetermination of mercury with diethyldithiocarbamate in excesses of metals ethylenediaminetetraacetate solutions. Anal Chim Acta. 1956;14:339–43.
52. Bobtelsky M, Rafailoff R. A precise direct heterometric determination of traces of copper with diethyldithiocarbamate in excesses of metals. Anal Chim Acta. 1956;14:558–67.
53. Urbowicz G, Krysiak A, Lulek J. Application of the silver diethyldithiocarbamate spectrophotometric method to determine total arsenic in some mineral waters. Bromatol Chem Toksykol. 2005;38(3):247.
54. Mousavi M, Hashemi A, Arjmand O, Amani AM, Babapoor A, Fateh MA, et al. Erythrosine adsorption from aqueous solution via decorated graphene oxide with magnetic iron oxide nano particles: kinetic and equilibrium studies. Acta Chim Slov. 2018;65(4):882–94.
55. Mousavi SM, Hashemi SA, Amani AM, Esmaeili H, Ghasemi Y, Babapoor A, et al. Pb (II) removal from synthetic wastewater using Kombucha Scoby and graphene oxide/Fe3O4. Physical Chemistry Research. 2018;6(4):759–71.
56. Mousavi SM, Hashemi SA, Esmaeili H, Amani AM, Mojoudi F. Synthesis of Fe3O4 nanoparticles modified by oak shell for treatment of wastewater containing Ni (II). Acta Chim Slov. 2018;65(3):750–6.
57. Bahrani S, Razmi Z, Ghaedi M, Asfaram A, Javadian H. Ultrasound-accelerated synthesis of gold nanoparticles modified choline chloride functionalized graphene oxide as a novel sensitive bioelectrochemical sensor: optimized meloxicam detection using CCD-RSM design and application for human plasma sample. Ultrason Sonochem. 2018;42:776–86. https://doi.org/10.1016/j.ultsonch.2017.12.042.
58. Xie G, Xi P, Liu H, Chen F, Huang L, Shi Y, et al. A facile chemical method to produce superparamagnetic graphene oxide–Fe 3 O 4 hybrid composite and its application in the removal of dyes from aqueous solution. J Mater Chem. 2012;22(3):1033–9.
59. Ai L, Zhang C, Chen Z. Removal of methylene blue from aqueous solution by a solvothermal-synthesized graphene/magnetite composite. J Hazard Mater. 2011;192(3):1515–24.
60. Cao H, Zhou X, Zhang Y, Chen L, Liu Z. Microspherical polyaniline/graphene nanocomposites for high performance supercapacitors. J Power Sources. 2013;243:715–20.
61. Wang L, Chen L, Yan B, Wang C, Zhu F, Jiang X, et al. In situ preparation of SnO 2@ polyaniline nanocomposites and their synergetic structure for high-performance supercapacitors. J Mater Chem A. 2014;2(22):8334–41.
62. Pang H, Huang C, Chen J, Liu B, Kuang Y, Zhang X. Preparation of polyaniline–tin dioxide composites and their application in methanol electro-oxidation. J Solid State Electrochem. 2010;14(2):169.
63. Xu XH, Ren GL, Cheng J, Liu Q, Li DG, Chen Q. Self-assembly of polyaniline-grafted chitosan/glucose oxidase nanolayered films for electrochemical biosensor applications. J Mater Sci. 2006;41(15):4974–7.

64. Han MG, Cho SK, Oh SG, Im SS. Preparation and characterization of polyaniline nanoparticles synthesized from DBSA micellar solution. Synth Met. 2002;126(1):53–60.
65. Jafari MJ. Application of vibrational spectroscopy in organic electronics: 2017-11-17, Planck, F-House, Campus Valla, Linköping, 10:15 (English): Linköping University Electronic Press. 2017, 61
66. Zacca M-J, Laurencin D, Richeter S, Clément S, Mehdi A. New layered polythiophene-silica composite through the self-assembly and polymerization of thiophene-based silylated molecular precursors. Molecules. 2018;23(10):2510.
67. Silva A, Ugucion J, Correa S, Ardisson J, Macedo W, Silva J, et al. Synthesis and characterization of nanocomposites consisting of polyaniline, chitosan and tin dioxide. Mater Chem Phys. 2018;216:402–412.
68. Yu T, Zhu P, Xiong Y, Chen H, Kang S, Luo H, et al. Synthesis of microspherical polyaniline/graphene composites and their application in supercapacitors. Electrochim Acta. 2016;222:12–9.
69. Palsaniya S, Nemade HB, Dasmahapatra AK. Synthesis of polyaniline/graphene/MoS2 nanocomposite for high performance supercapacitor electrode. Polymer. 2018;150:150–8.
70. Kumar S, Lei Y, Alshareef NH, Quevedo-Lopez MA, Salama KN. Biofunctionalized two-dimensional Ti3C2 MXenes for ultrasensitive detection of cancer biomarker. Biosens Bioelectron. 2018;121:243–9. https://doi.org/10.1016/j.bios.2018.08.076.
71. Bagheri H, Afkhami A, Khoshsafar H, Rezaei M, Shirzadmehr A. Simultaneous electrochemical determination of heavy metals using a triphenylphosphine/MWCNTs composite carbon ionic liquid electrode. Sensors Actuators B Chem. 2013;186:451–60. https://doi.org/10.1016/j.snb.2013.06.051.
72. Wang N, Lin M, Dai H, Ma H. Functionalized gold nanoparticles/reduced graphene oxide nanocomposites for ultrasensitive electrochemical sensing of mercury ions based on thymine-mercury-thymine structure. Biosens Bioelectron. 2016;79:320–6. https://doi.org/10.1016/j.bios.2015.12.056.
73. Liu W, Wu X, Li X. Gold nanorods on three-dimensional nickel foam: a non-enzymatic glucose sensor with enhanced electrocatalytic performance. RSC Adv. 2017;7(58):36744–9. https://doi.org/10.1039/c7ra06909j.